

# Implementation of a finite-amplitude method in a relativistic meson-exchange model

Xuwei Sun and Dinghui Lu

*Department of Physics, Zhejiang University, 310027 Hangzhou, China*

(Received 2 June 2017; revised manuscript received 21 July 2017; published 21 August 2017)

The finite-amplitude method is a feasible numerical approach to large scale random phase approximation calculations. It avoids the storage and calculation of residual interaction elements as well as the diagonalization of the RPA matrix, which will be prohibitive when the configuration space is huge. In this work we finished the implementation of a finite-amplitude method in a relativistic meson exchange mean field model with axial symmetry. The direct variation approach makes our FAM scheme capable of being extended to the multipole excitation case.

DOI: [10.1103/PhysRevC.96.024614](https://doi.org/10.1103/PhysRevC.96.024614)

## I. INTRODUCTION

Random phase approximation (RPA) and its generalization, quasiparticle random phase approximation (QRPA) method, are important tools to investigate the low lying excitation properties of nuclei both stable and far from the stability line. However, under axial symmetry, the configuration space of “particle-hole” pairs grows rapidly such that it prohibits the calculation and storage of residual interaction matrix elements as well as the diagonalization. Therefore the nonspherical applications are limited in light and medium nuclei [1–5]; otherwise various truncations have to be introduced, such as the energy cutoffs of particle-hole (p-h) pairs, occupation probabilities, major shell numbers, etc., which hampers the self-consistency of the calculation scheme itself. To circumvent the deficiencies of a conventional implementation of the QRPA through diagonalization, Nakatsukasa *et al.* [6] developed the finite-amplitude method (FAM) wherein the variation of the Hamiltonian is calculated numerically through finite difference. The numerical costs of the FAM increase linearly with the dimension of configuration space, which enables the RPA/QRPA calculation of super-heavy nuclei without spherical symmetry restriction. The feasibility of the FAM makes this new numerical approach widely used in recent RPA/QRPA calculations. The application of the FAM in the nonrelativistic Skyrme random phase approximation model has been fulfilled both without pairing [7–9] and with pairing [10,11] interactions. In the relativistic mean-field (RMF) area, a FAM based on the relativistic point coupling model with parameter set DD-PC1 [12] has been built by Liang *et al.* [9] under spherical symmetry and by T. Nikšić *et al.* [13] under axial symmetry. However the implementation in the relativistic meson-exchange model has not been established yet.

The nuclear density functional theory (DFT) [14] is highly developed and nowadays a lot of computing programs have been fulfilled, well checked, and are open access. One benefit of the FAM is that the implementation can take the most advantage of the corresponding static DFT solver. Therefore, many finite-amplitude method implementations are carried out by extending ground state code.

The code HOSPHE [15] is the self-consistent solution to the effective functional  $N^3\text{LO}$  [16], which contains a high order of gradient corrections within the local density

approximation. Carlsson *et al.* have used this code to perform FAM-QRPA calculations in the spherical symmetry condition [17]. The widely used axial deformed nonrelativistic Skyrme-HFB solver HFBTHO [18,19] has also been extended to the FAM-QRPA scheme in several studies [11,20,21]. The preceding two solvers expand single-particle wave functions with a harmonic oscillator basis, while there are other types using space coordinate representation. For example, HFBRAD [22] is a code fulfilled in a coordinate representation using a spherical box, finite-amplitude method implementation of the Skyrme-QRPA based on this program also have been completed [10,23]. HFB-AX [24] is a two-dimensional lattice Skyrme-HFB solver; a FAM-QRPA has been built based on this deformed coordinate-space program concerning continuum states [25].

In fact, the FAM has shown excellent performance, a systematic study about pygmy dipole resonance in a wide range of nuclei without assumed symmetry has been carried out through a Skyrme-FAM-RPA [8]. It’s also been applied in the investigation of charge changing excitation, e.g., Mustonen *et al.* have applied a proton-neutron FAM [26] scheme in the estimation of  $\beta$ -decay rates in axially deformed open-shell nuclei.

As a realization of linear response theory, in the FAM the excited eigenmodes are not directly provided. The transition strength caused by an external field at a given frequency is obtained after solving the linear response equation iteratively. Sometimes one may be interested about the discrete eigenstates. Hinohara *et al.* has shown that the eigenmode can be accessed through performing a contour integral in the complex frequency plane around QRPA poles [20]. Besides the iteration FAM(i-FAM), the idea of finite difference can also be used to calculate the matrix elements of a residual interaction. Avogadro *et al.* have built the matrix FAM(m-FAM) [23] scheme, wherein the matrix elements of a residual interaction are evaluated by constructing Hamiltonian variation from a particular particle-hole transition, and then the eigenvalues and vectors are obtained by diagonalizing RPA equations. If the dimension of configuration space is less than ten thousand, the m-FAM even has a better performance than the i-FAM.

The relativistic mean field theory is covariant and self-consistent; it introduces the spin freedom naturally and

can explain pseudospin symmetry elegantly. The interaction between nucleons are interpreted as exchanging scalar  $\sigma$ , vector  $\omega$  meson, and isospin vector meson  $\rho$  as well as photon for electromagnetic interaction. Implementation of a FAM in a relativistic meson-exchange model can provide a practical approach for systematic researching the low-lying excitation properties of open-shell nuclei.

This paper is organized as follows: first we introduce the general framework of the finite-amplitude method, and then construct the variation of the Hamiltonian within the relativistic meson-exchange mean field theory. Second, the numerical details are shown, including the decoupling of spurious states and benchmarking with the existing theoretical calculation result. In the third part, we apply our method to the study of the breathing mode in even-even cadmium isotopes and electric dipole excitation in  $^{60}\text{Ni}$ . Last, conclusion and remarks are given.

## II. FORMALISM

### A. The general framework of a finite-amplitude method

In the Hartree-Bogoliubov theory, the generalized single particle Hamiltonian can be obtained from the variation of the energy density functional

$$\mathcal{H} = \frac{\partial E[\mathcal{R}]}{\partial \mathcal{R}} = \begin{pmatrix} h & \Delta \\ -\Delta^* & -h^* \end{pmatrix}, \quad (1)$$

where  $\mathcal{R}$  is the generalized density,  $h$  and  $\Delta$  are the single particle Hamiltonian and the pairing field [27,28]. The variation of the generalized Hamiltonian in quasiparticle space is connected with that in oscillator space by

$$\begin{pmatrix} \delta H^{11} & \delta H^{20} \\ \delta H^{02} & -\delta H^{11T} \end{pmatrix} = \mathcal{W}^\dagger \begin{pmatrix} \delta h & \delta \Delta \\ -\delta \Delta^* & -\delta h^T \end{pmatrix} \mathcal{W}, \quad (2)$$

where the transformation matrix reads [28]

$$\mathcal{W} = \begin{pmatrix} U & V^* \\ V & U^* \end{pmatrix}. \quad (3)$$

The evolution of the generalized density matrix satisfies the time-dependent Hartree-Fock-Bogoliubov equation (TDHFB) [28]

$$i \partial_t \mathcal{R}(t) = [\mathcal{H}(t) + \mathcal{F}(t), \mathcal{R}(t)]. \quad (4)$$

The ground state of the HFB is a quasiparticle vacuum, which means, in the quasiparticle space we have

$$\mathcal{R}_0 = \begin{pmatrix} 0 & 0 \\ 0 & 1 \end{pmatrix}, \quad \mathcal{H}_0 = \begin{pmatrix} E & 0 \\ 0 & -E \end{pmatrix}. \quad (5)$$

When the nucleus is perturbed by an external field  $\hat{F}$  with a frequency  $\omega$ ,

$$\hat{F}(t) = \hat{F} e^{-i\omega t} + \text{H.c.} \quad (6)$$

The elements of  $\hat{F}$  in generalized quasiparticle space are similar to (2):

$$\begin{pmatrix} F^{11} & F^{20} \\ F^{02} & -F^{11T} \end{pmatrix} = \mathcal{W}^\dagger \begin{pmatrix} f & 0 \\ 0 & -f^T \end{pmatrix} \mathcal{W}. \quad (7)$$

In the small amplitude limit, the induced density is

$$\mathcal{R} = \mathcal{R}_0 + \delta \mathcal{R} e^{-i\omega t} + \text{H.c.} \quad (8)$$

As a projector operator, the generalized density satisfies  $\mathcal{R}^2 = \mathcal{R}$ , which means the nonvanishing elements of the transition density are

$$\delta \mathcal{R} = \begin{pmatrix} 0 & \delta R^{20} \\ \delta R^{02} & 0 \end{pmatrix} := \begin{pmatrix} 0 & X \\ Y & 0 \end{pmatrix}. \quad (9)$$

Substituting the above expressions into (4), we can obtain the linear response equation

$$\begin{aligned} (E_\mu + E_\nu - \omega) X_{\mu\nu}(\omega) + \delta H_{\mu\nu}^{20}(\omega) &= -F_{\mu\nu}^{20}(\omega), \\ (E_\mu + E_\nu + \omega) Y_{\mu\nu}(\omega) + \delta H_{\mu\nu}^{02}(\omega) &= -F_{\mu\nu}^{02}(\omega). \end{aligned} \quad (10)$$

In conventional RPA/QRPA calculations, the variations of Hamiltonian  $\delta H^{20}$  and  $\delta H^{02}$  are further expanded with transition density  $X, Y$  and residual interaction matrix elements, and then one gets the coupled equations of  $X, Y$ , i.e., the RPA/QRPA equation. However, in the finite-amplitude method, the start point is (10);  $\delta H^{20}$  and  $\delta H^{02}$  are calculated directly from finite difference.

The kernel of the FAM is to construct  $\delta h$ ,  $\delta \Delta$ , and  $\delta \Delta^*$  without calculating the matrix elements of the residual interaction. The use of small parameter  $\eta$  [6,7,11,23] enables one to extract the single particle Hamiltonian variation from finite difference

$$\delta \hat{h} = \frac{\hat{h}[\hat{\rho}_0 + \eta \delta \hat{\rho}] - \hat{h}[\hat{\rho}_0]}{\eta}. \quad (11)$$

In this scheme, one can take advantage of the subroutine  $\hat{h}[\hat{\rho}]$  of the original code; usually only a minimal modification is needed. The real parameter  $\eta$  should be chosen carefully; if the value is too large, the finite difference is inaccurate, but  $\eta$  should not be too small either; otherwise the iteration will suffer from significant numerical noise [7,13].

To address this problem from another point of view, we adopt an approach of direct variation instead of finite difference, namely, fulfill a subroutine  $\delta \hat{h}[\hat{\rho}_0, \delta \hat{\rho}]$  responsible for calculating variation of the Hamiltonian from transition densities. Of course, the structure of  $\delta \hat{h}$  is much more complex than  $\hat{h}$ , which usually contains higher orders of derivatives. However, it frees us from the choosing of  $\eta$  and what's more, is convenient to be applied in the  $K^\pi \neq 0^+$  case. The similar scheme has also been adopted in the Skyrme-FAM-QRPA implemented by Kortelainen *et al.* [21], which are intended to research the multipole excitations of axially deformed superfluid nuclei.

### B. Variation of the Hamiltonian in the relativistic meson-exchange model

In the relativistic meson-exchange mean field theory, the single particle Dirac equation is [29]

$$[\gamma^\mu (i \partial_\mu + V_\mu) + (M + S)] \psi = 0, \quad (12)$$

where the scalar and vector potential are generated from exchanging mesons and photon:

$$S = g_\sigma \sigma, \quad (12)$$

$$V_\mu = g_\omega \omega_\mu + g_\rho \vec{\rho}_\mu \cdot \vec{\tau} + \frac{1 - \tau_3}{2} \cdot e A_\mu + \Sigma_{\mu(R)}. \quad (13)$$

The last ingredient of the vector potential is the ‘‘rearrangement’’ term [30]; it appears when the coupling constants are density dependent. At the mean field level, due to time-reversal symmetry, the space components of a meson field are vanished, and there’s no mixing in the isospin space, i.e., only the third component of an isospin-vector meson contributes. The evolution of meson fields satisfy the Klein-Gordon equation

$$\begin{aligned} (-\Delta + m_\sigma^2)\sigma(\mathbf{r}) &= -g_\sigma \rho_s(\mathbf{r}), \\ (-\Delta + m_\omega^2)\omega(\mathbf{r}) &= +g_\omega \rho_v(\mathbf{r}), \\ (-\Delta + m_\rho^2)\rho(\mathbf{r}) &= +g_\rho \rho_{tv}(\mathbf{r}), \\ -\Delta A(\mathbf{r}) &= +e\rho_c(\mathbf{r}), \end{aligned} \quad (14)$$

where the distribution of the scalar/vector density and isospin-vector density as well as the charge density are defined by

$$\begin{aligned} \rho_s(\mathbf{r}) &= \text{Tr}[\beta \hat{\rho}], \quad \rho_v(\mathbf{r}) = \text{Tr}[\hat{\rho}], \\ \rho_{tv}(\mathbf{r}) &= \text{Tr}[\tau_3 \hat{\rho}], \quad \rho_c(\mathbf{r}) = \frac{1}{2} \text{Tr}[(1 - \tau_3) \hat{\rho}]. \end{aligned} \quad (15)$$

When the nuclei are disturbed by an external field, the varying of the scalar and vector potential will induce the variation of the Hamiltonian

$$\delta \hat{h} = -\boldsymbol{\alpha} \delta \mathbf{V} + \delta V + \beta \delta S = \begin{pmatrix} \delta V + \delta S & -\boldsymbol{\sigma} \cdot \delta \mathbf{V} \\ -\boldsymbol{\sigma} \cdot \delta \mathbf{V} & \delta V - \delta S \end{pmatrix}, \quad (16)$$

where the scalar potential variation as well as the time and space component of the vector potential variation are

$$\begin{aligned} \delta S &= g_\sigma^0 \delta \sigma + \delta g_\sigma \sigma^0, \\ \delta V &= g_\omega^0 \delta \omega + \delta g_\omega \omega^0 + g_\rho^0 \delta \boldsymbol{\rho} \cdot \boldsymbol{\tau}_3 + \delta g_\rho \boldsymbol{\rho}^0 \cdot \boldsymbol{\tau}_3 \\ &\quad + \frac{1 - \tau_3}{2} \cdot \delta V_c + \delta \Sigma_{0(R)}, \\ \delta \mathbf{V} &= g_\omega^0 \delta \boldsymbol{\omega} + g_\rho^0 \delta \boldsymbol{\rho} \cdot \boldsymbol{\tau}_3. \end{aligned} \quad (17)$$

The quantities labeled by ‘‘0’’ are coupling constants and meson fields belonging to the unperturbed ground state. What is worthy to mention here is that the space components of the vector potential are vanished in the ground state of even-even nuclei; however, in order to calculate the excitation behavior, the current contributions should be included. Neglecting the spatial components of the vector field will push the giant monopole peak about 2 MeV higher [31].

Under axial symmetry condition, the total angular momentum  $\mathbf{J}$  is no longer a good quantum number, but the projection of angular momentum on the  $z$  axis and the parity are still conserved. The excitation of a nucleus can be studied in different  $K$  channels, which to some extent, reduces the dimension of configuration space. Therefore, if the nucleus is perturbed by the external field operator  $\hat{Q}_{IK}$ , then in the linear limit, the variation of densities will have an azimuthal dependence like [5]

$$\delta \rho_m(\mathbf{r}) = \delta \rho_m(r_\perp, z) e^{-iK\varphi}. \quad (18)$$

Here,  $m$  represents scalar, vector, isospin vector, and charge densities. It can be proved that the variation of meson fields has the same azimuthal dependence as the densities. Under the small amplitude limit the variation of the meson field can be calculated through the Klein-Gordon equation

$$(-\Delta + m_m^2) \delta \phi_m(\mathbf{r}) = \mp \left[ g_m^0(\mathbf{r}) \delta \rho_m(\mathbf{r}) + \frac{\partial g_m}{\partial \rho_v} \delta \rho_v(\mathbf{r}) \rho_m^0(\mathbf{r}) \right]. \quad (19)$$

After dealing with the azimuthal part analytically, the above equation can be calculated by expanding the meson field and source at the right hand side with harmonic oscillator wave functions, namely,

$$\delta \phi_m(r_\perp, z) = \sum_\alpha^{N_B} f_\alpha \phi_\alpha^K(r_\perp, z) \quad (20)$$

$$\begin{aligned} &\mp \left[ g_m^0 \delta \rho_m(r_\perp, z) + \frac{\partial g_m}{\partial \rho_v} \delta \rho_v(r_\perp, z) \rho_m^0 \right] \\ &= \sum_\alpha^{N_B} s_\alpha^m \phi_\alpha^K(r_\perp, z), \end{aligned} \quad (21)$$

where  $\phi_\alpha^K$  is the cylindrical oscillator basis

$$\phi_\alpha^K(r_\perp, z) = \phi_{n_r}^K(r_\perp) \phi_{n_z}(z). \quad (22)$$

The explicit expression of the deformed harmonic oscillator basis is listed in Appendix A. The equation (19) in such a basis becomes

$$\sum_{\alpha'}^{N_B} M_{\alpha'\alpha} f_{\alpha'} = s_\alpha^m, \quad (23)$$

with

$$\begin{aligned} M_{\alpha'\alpha} &= \int dz \int r_\perp dr_\perp \phi_{\alpha'}^K \left[ -\Delta^a + \frac{K^2}{r_\perp^2} + m_m^2 \right] \phi_\alpha^K \\ &= -2\delta_{n'_z, n_z} \int_0^\infty d\eta \phi_{n'_r}^K \left( \frac{\partial}{\partial \eta} + \eta \frac{\partial^2}{\partial \eta^2} \right) \phi_{n_r}^K \\ &\quad - \frac{1}{b_z} \delta_{n'_r, n_r} \int_{-\infty}^\infty d\zeta \phi_{n'_z}^K \frac{\partial^2}{\partial \zeta^2} \phi_{n_z} + \frac{K^2}{2} \delta_{n'_z, n_z} \\ &\quad \times \int_0^\infty d\eta \phi_{n'_r}^K \eta^{-1} \phi_{n_r}^K + m_m^2 \delta_{n'_z, n_z} \delta_{n'_r, n_r}, \end{aligned} \quad (24)$$

where  $\Delta^a$  is the azimuthal independent part of the Laplace operator.

The Coulomb field is long range, singular at the origin; therefore it can not be expanded in an oscillator basis; the method used for meson fields fails. In this case the standard Green function method should be adopted [32]:

$$V_c(\mathbf{r}) = \frac{e}{4\pi} \int d^3 \mathbf{r}' \frac{\rho_c(\mathbf{r}')}{|\mathbf{r} - \mathbf{r}'|}. \quad (25)$$

The relative distance in the numerator is singular when  $\mathbf{r} = \mathbf{r}'$ , which is inconvenient for numerical calculation and should be avoided by using the relation

$$\Delta_{\mathbf{r}'} |\mathbf{r} - \mathbf{r}'| = \frac{2}{|\mathbf{r} - \mathbf{r}'|}. \quad (26)$$

After integration by parts twice, the equation (25) becomes

$$V_c(\mathbf{r}) = \frac{e}{8\pi} \int d^3\mathbf{r}' |\mathbf{r} - \mathbf{r}'| \Delta \rho_c(\mathbf{r}'). \quad (27)$$

In a small amplitude approximation, the variation of the Coulomb potential can be obtained similarly as

$$\delta V_c(\mathbf{r}) = \frac{e}{8\pi} \int d^3\mathbf{r}' |\mathbf{r} - \mathbf{r}'| \Delta \delta \rho_c(\mathbf{r}'), \quad (28)$$

while from (18) we can see that the second variation of  $\delta \rho_c$  has an extra azimuthal dependent form:

$$\Delta \delta \rho_c(\mathbf{r}) = e^{-iK\varphi} \left( \Delta^a - \frac{K^2}{r_\perp^2} \right) \delta \rho_p(r_\perp, z). \quad (29)$$

Substitute this into (28) leads to

$$\begin{aligned} \delta V_c(\mathbf{r}) &= \frac{e}{4\pi} (-1)^K e^{-iK\varphi} \int_0^\infty r'_\perp dr'_\perp \int_{-\infty}^\infty dz' \\ &\times [(z - z')^2 + (r_\perp + r'_\perp)^2]^{1/2} \\ &\times \left( \Delta^a - \frac{K^2}{r'_\perp{}^2} \right) \delta \rho_c(r'_\perp, z') \\ &\times I^K \left[ \frac{4r_\perp r'_\perp}{(z - z')^2 + (r_\perp + r'_\perp)^2} \right]. \end{aligned} \quad (30)$$

The expression above leaves us the problem to evaluate the integral

$$I^K(x) = \int_0^\pi \sqrt{1 - x \sin^2 \theta} \cos(2K\theta) d\theta. \quad (31)$$

In the case of  $K = 0$  and  $K = 1$ ,  $I^K$  can be expressed as elliptic integrals. While in  $K > 1$  case, we calculate a series of values  $I_i^K$  at  $x_i$  numerically, and introduce a quadratic interpolation procedure to get the function  $I^K(x)$ . We have tested the performance of such a treatment; the result is satisfying.

If the coupling constants are density dependent, there's a rearrangement term contributing to the vector potential

$$\Sigma_0^R = \frac{\partial g_\sigma}{\partial \rho_v} \rho_s \sigma + \frac{\partial g_\omega}{\partial \rho_v} \rho_v \omega + \frac{\partial g_\rho}{\partial \rho_v} \rho_{tv} \rho. \quad (32)$$

The variation of the rearrangement term is somewhat complex because when density varies, the three parts, namely, the derivative of the coupling constant, the meson field, and the scalar, vector, vector-isovector density, all change accordingly. Under linear approximation, the variation of the rearrangement term originates from three aspects:

$$\begin{aligned} \delta \Sigma_0^R(\mathbf{r}) &= \sum_m \left\{ \frac{\partial^2 g_m(\mathbf{r})}{\partial \rho_v^2} \Big|_0 \delta \rho_v(\mathbf{r}) \rho_m^0(\mathbf{r}) \phi_m^0(\mathbf{r}) \right. \\ &\left. + \frac{\partial g_m(\mathbf{r})}{\partial \rho_v} \Big|_0 \delta \rho_m(\mathbf{r}) \phi_m^0(\mathbf{r}) + \frac{\partial g_m(\mathbf{r})}{\partial \rho_v} \Big|_0 \rho_m^0(\mathbf{r}) \delta \phi_m(\mathbf{r}) \right\}. \end{aligned} \quad (33)$$

The subscript 0 in the right hand side means the expression is valued with the ground state. It's not difficult to see that the variation of rearrangement carries an azimuth factor  $e^{-iK\varphi}$  because the three variations at the right hand side (rhs) of

Eq. (33) all carry such a one while quantities valued in the ground state are all azimuthally independent.

Because in the ground state of even-even nuclei the currents vanish, the Klein-Gordon equations involving spatial components of vector meson  $\delta \boldsymbol{\omega}$  and the third component of isovector-vector meson  $\delta \boldsymbol{\rho}$  differ from (19), that is,

$$\begin{aligned} (-\Delta + m_\omega^2) \delta \boldsymbol{\omega}(\mathbf{r}) &= g_\omega(\mathbf{r}) \mathbf{j}(\mathbf{r}), \\ (-\Delta + m_\rho^2) \delta \boldsymbol{\rho}(\mathbf{r}) &= g_\rho(\mathbf{r}) \mathbf{j}^T(\mathbf{r}), \end{aligned} \quad (34)$$

where  $\mathbf{j}$  and  $\mathbf{j}^T$  are the vector and the isovector current, respectively. ( $\mathbf{j}$  and  $\mathbf{j}^T$  are aroused by external perturbation). The equation above can be solved with the method that has been developed in the preceding context.

Once the variation of the meson field is obtained, it is a straightforward thing to get the variation of the single particle Hamiltonian from (16). The variation of coupling parameters is trivial; therefore we put them in Appendix B as well as the explicit form about the density dependence of coupling constants.

For a good description of open-shell nuclei, the inclusion of pairing interaction is necessary. The pairing field is a functional of the abnormal tensor  $\hat{\kappa}$ :

$$\hat{\Delta} = \frac{1}{2} \text{Tr}(V^{PP} \hat{\kappa}). \quad (35)$$

When the pairing interaction is density independent, in the linear approximation the variation of the pairing field can be easily obtained through

$$\delta \hat{\Delta} = \frac{1}{2} \text{Tr}(V^{PP} \delta \hat{\kappa}). \quad (36)$$

Although there's some attempts to handle the pairing effect from a relativistic view [33], it is still an open question about the relativistic structure of the pairing field so far. Therefore, it's customary to use a hybrid model wherein the relativistic interaction provide a covariant mean field while the pairing interaction is handled with a nonrelativistic Skyrme or Gogny force [34]. In our study, a separable form of the Gogny force has been adopted [35]:

$$\begin{aligned} V^{PP}(\mathbf{r}_1, \mathbf{r}_2, \mathbf{r}'_1, \mathbf{r}'_2) &= -G \delta(\mathbf{R} - \mathbf{R}') P(\mathbf{r}) P(\mathbf{r}') \\ &\times (1 - P^\sigma)/2. \end{aligned} \quad (37)$$

Here  $\mathbf{R}$  and  $\mathbf{r}$  denote the center-of-mass and relative coordinates, respectively, and  $\mathbf{r}_i$  are particle coordinates in the intrinsic frame.  $P(\mathbf{r})$  is in the form of a Gaussian function, which makes the pairing force converge quickly. The spin projector operator  $(1 - P^\sigma)/2$  restricts the pairing interaction effects only between  $S = 0$  pairs. The deformed oscillator basis in these two sets of coordinate frames can be transformed to each other through Talmi-Moshinsky brackets [36,37]. The matrix elements of the pairing interaction in harmonic oscillator space can be expressed as a sum of separable terms [34,35]

$$\langle \alpha\beta | V^{PP} | \gamma\delta \rangle = -G \sum_N W_{\alpha\beta}^{N*} W_{\gamma\delta}^N. \quad (38)$$

Therefore the matrix elements of pairing potential variation can be easily calculated from (36)

$$\delta\Delta_{\alpha\beta} = -G \sum_N \tilde{P}_N W_{\alpha\beta}^{N*}, \quad (39)$$

with

$$\tilde{P}_N = \frac{1}{2} \text{Tr}(W^N \delta\kappa). \quad (40)$$

### C. The transition strength

Solving the linear response equation (10) will give us the transition density  $X(\omega), Y(\omega)$ , from which the transition strength will be accessible. In quasiparticle space it reads [10]

$$\frac{dB(F, \omega)}{d\omega} = -\frac{1}{2\pi} \text{Im} \sum_{\mu\nu} \{F_{\mu\nu}^{20*} X_{\mu\nu}(\omega) + F_{\mu\nu}^{02*} Y_{\mu\nu}(\omega)\}. \quad (41)$$

The imaginary part  $i\gamma$  added in  $\omega$  is equivalent to a smear strength function with the Lorentzian width  $\Gamma = 2\gamma$ ; therefore, the integral over strength distribution gives the same  $k$ th energy weighed sum rule (EWSR) as calculated via discrete eigenmodes,

$$m_k = \sum_{\nu} \omega_{\nu}^k B(F, \omega_{\nu}) = \int \omega^k \frac{dB(F, \omega)}{d\omega} d\omega. \quad (42)$$

## III. NUMERICAL DETAILS

The effective functional used in our implementation is the relativistic density-dependent meson-exchange model with parameter set DD-ME2 [38], while in the pairing channel, a separable form of the Gogny force [35,39] is adopted. Instead of extending the ground subroutines, we use the ground quasiparticle wave functions  $U, V$  of code DIRHB [34] as inputs, where the wave functions of quasiparticle as well as the meson fields are expanded with deformed harmonic oscillators in cylindrical coordinates, and then establish the finite-amplitude method framework independently.

The linear response function (10) is solved iteratively, which starts from a guess about transition density  $X_0, Y_0$ . In the first step of each iteration, the transition density is transformed from quasiparticle space to oscillator space via

$$\begin{pmatrix} \delta\rho & \delta\kappa \\ -\delta\bar{\kappa}^* & -\delta\rho^* \end{pmatrix} = \mathcal{W} \begin{pmatrix} 0 & X \\ Y & 0 \end{pmatrix} \mathcal{W}^\dagger. \quad (43)$$

Then the variation of single particle Hamiltonian  $\delta h$  and pairing potential  $\delta\Delta, \delta\bar{\Delta}^*$  are calculated through the direct variation procedure introduced in the previous section. These terms are transformed back to quasiparticle space via (2) and one gets  $\delta H^{20}$  and  $\delta H^{02}$ . The new transition density  $X', Y'$  can be obtained from (10), namely,

$$X'_{\mu\nu} = \frac{\delta H_{\mu\nu}^{20} + F_{\mu\nu}^{20}}{E_{\mu} + E_{\nu} - \omega}, \quad Y'_{\mu\nu} = \frac{\delta H_{\mu\nu}^{02} + F_{\mu\nu}^{02}}{E_{\mu} + E_{\nu} + \omega}, \quad (44)$$

which is the last step of each iteration. To avoid the singularity, the frequency  $\omega$  is added with an imaginary part  $\gamma$ . The convergence criterion is chosen as follows: if the length of residua between input vector  $(X, Y)$  and output one  $(X', Y')$  is  $10^{-8}$  times less than the length of the input vector, the

TABLE I. The relationship between the configuration space dimension and the maximum major quantum number of oscillator shells in the  $K^{\pi} = 0^+$  channel.

$N_F$	8	10	12	14	16
$N_{2qp}$	12 857	30 678	64 349	122 670	217 225

iteration stops. In order to accelerate the iteration, we adopt the algorithm of the Broyden mixing method [40,41]; in this way the averaged iterations needed to converge can be reduced to about 40 times. The responses of a system at different frequency  $\omega$  are independent and can be easily deployed in a message passing interface (MPI) parallel environment, which is beneficial for systematic calculations.

In our calculation scheme, the amount of total quasiparticle states changes with the major quantum number  $N_F$ . The configuration space of two quasiparticle (2qp) pairs increases with  $N_F$  rapidly. For instance, in the  $K^{\pi} = 0^+$  channel, the 2qp pairs  $(\mu, \nu)$  are constructed from the configuration requirement  $\Omega_{\mu} + \Omega_{\nu} = 0$ ,  $\pi_{\mu}\pi_{\nu} = +$ , and reduced by half from the condition  $\mu > \nu$  due to exchange symmetry. If ten major shells are used, the number of 2qp pairs will exceed thirty thousand when no further truncations on quasiparticle states are made and all antiquasiparticle pairs are included. We summarized the relationship between the number of 2qp pairs and  $N_F$  in this channel and list the result in Table I.

It's interesting to notice that the increase of configuration space with major quantum number can be well approximated as

$$N_{2qp} \approx 1.849(N_F)^{4.21}, \quad (45)$$

with goodness of fit  $R^2 = 0.9999$ .

In the oscillator representation, the quasiparticle states in continuum are approximated by discrete levels; for this reason, although the bound states will remain constant, the effects of continuum spectrum have a dependence on  $N_F$ . As a result, when  $N_F$  changes, the strength function in the high energy region will shift slightly, because states in continuum play important roles. While in the low energy region, the 2qp pairs formed by bound states dominate, the transition strength remains unchanged. Our tests show that  $N_F = 16$  is enough to make most calculations converge; further increase of  $N_F$  only brings in insignificant corrections. In this case, the 2qp number is roughly two hundred thousand, which means over  $4 \times 10^{10}$  residual matrix elements should be calculated and stored; that is definitely out of the reach of conventional RPA/QRPA calculations through diagonalization.

A fully self-consistent quasiparticle random phase approximation procedure will restore the symmetry broken by the mean field calculation. The decoupling of spurious states can be used to verify the accuracy of numerical implementation. In Fig. 1 we display our calculation about the giant monopole resonance in light nuclei  $^{22}\text{O}$ . The dotted-dashed line represents the situation without dynamic pairing [13], which means the pairing correlation is involved in the ground state but omitted in the excitation calculation. From Fig. 1 it's clear to see that when the pairing interaction is not included consistently, there

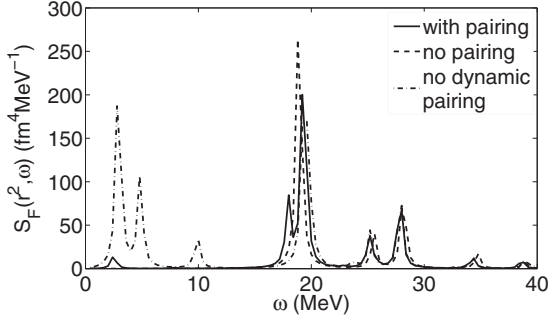


FIG. 1. The elimination of a spurious state relating to particle number symmetry breaking in the  $K^\pi = 0^+$  channel. The figure shows the giant monopole resonance of  $^{22}\text{O}$ ; the dashed line represents the result corresponding to the RMF-FAM-RPA calculation, while the solid line for the self-consistent RMF-FAM-QRPA. The dotted-dashed line shows the mixing of the spurious state with physical ones when dynamic pairing is not included, namely, omitting the pairing interaction in the excitation calculations; see text for details.

are significant spurious states in the low-lying energy region. On the contrary, the solid line represent the case in which the pairing is self-consistently included; the mixing of the spurious state with physical ones is eliminated. When switching off the pairing interaction both in static as well as excitation calculations, the RMF-QRPA reduces to the RMF-RPA, which is the situation labeled by the dashed line. In this manner, the Nambu-Goldstone boson corresponding to particle-number symmetry broken in the  $K^\pi = 0^+$  channel will not appear. The discrepancy between the solid line and dashed one indicates the effect of the pairing correction on the monopole resonance, that is, the splitting of the main peak of the giant monopole resonance (GMR) at about 20 MeV.

We compared our calculation with the result of [13] about the same nucleus  $^{22}\text{O}$  while using a density-dependent point coupling model with parameter set DD-PC1. The behavior of the resonance strengths resembles each other, and in both cases there's the significant elimination of the spurious state when the pairing interaction is consistently considered. When the dynamic pairing is consistently included, our calculation shows that a small peak appears around 2–3 MeV. The same result has also been found in the canonical QRPA calculation [42] with a nonlinear meson-exchange interaction NL3. Recently, in the QRPA calculation based on point-coupling interaction DD-PC1, such a state is also reproduced both from diagonalization and a FAM scheme [13].

## IV. RESULT

### A. Monopole resonance of cadmium isotopes

The nuclear matter compressibility and the frequency of collective monopole resonance are closely correlated [43] and provide essential restriction on the equation of state for nuclear matter. As a first application of our FAM-QRPA implementation, we investigate the giant monopole resonance of cadmium even-even isotopes  $^{110-116}\text{Cd}$  in an axial symmetry scheme. The deformation of these nuclei change from 0.16 to

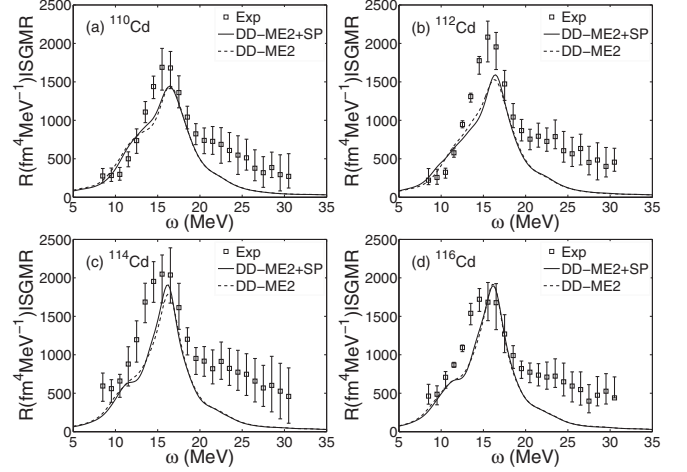


FIG. 2. The giant monopole resonance of Cd isotopes. The solid line represents the self-consistent FAM-QRPA calculation with the separable pairing (SP) force, while the dashed line represents the pairing-absent case. The experimental results are denoted by error bars.

0. The isoscalar monopole operator is [13]

$$\hat{F} = \sum_i r_i^2. \quad (46)$$

In Fig. 2 we compare our calculation with the experimental result [44] obtained by inelastic  $\alpha$  scattering. To reconcile with the experimental curves, the theoretical calculations are smeared with a relatively large width  $\Gamma = 3$  MeV.

In Fig. 2, we represent the isoscalar giant monopole resonance (ISGMR) strength distribution obtained in our FAM-QRPA calculation with solid lines, and represent the FAM-RPA results with dashed lines. In the latter cases the pairing interaction is omitted both in the static state and excitations. The overall effects of pairing in these cadmium isotopes are unremarkable, which to some extent make the GMR peaks more concentrated. Pairing corrections are not obvious when the excited energy is larger than about 15 MeV, where the excitations of nucleons far from the Fermi surface begin to make a more stronger contribution. In general, the theoretical calculations are in agreement with experimental results. However, in the energy region about 12–15 MeV, the theoretical predictions are lower than experimental data, partly because the calculated GMR structures locate higher.

In Table II, we compare the centroid energies of our calculation with experimental results as well as some relativistic and nonrelativistic random phase approximation method calculations. The prediction of our model, which combines the density-dependent covariant meson exchange interaction DD-ME2 and separable form of the Gogny force in the pairing channel, is larger than experimental data by about 0.8 MeV (although there's a conflict about 0.1 MeV on nucleus  $^{116}\text{Cd}$  in experiments [44] and [45], but both of them are well below theoretical predictions). We make a comparison of our results with the RPA calculations fulfilled by Patel *et al.* [44] with the relativistic nonlinear meson exchange models; our centroid energies lie between the values predicted by NL3 [46] and

TABLE II. Centroid energy ( $E_{\text{cen}} = m_1/m_0$ ) comparison of different theoretical models and experimental results in cadmium isotopes. Our calculation results are listed in the second column in MeV.

	This work	SkP	SkM*	Sly5	NL3	FSUGold	Expt. 1 [44]	Expt. 2 [45]
$^{110}\text{Cd}$	16.67	15.56	16.18	16.54	17.09	16.59	$15.94 \pm 0.07$	$15.71^{+0.11}_{-0.11}$
$^{112}\text{Cd}$	16.56	15.42	16.05	16.39	17.00	16.50	$15.80 \pm 0.05$	
$^{114}\text{Cd}$	16.44	15.28	15.91	16.25	16.90	16.38	$15.61 \pm 0.08$	
$^{116}\text{Cd}$	16.38	15.14	15.78	16.12	16.77	16.27	$15.44 \pm 0.06$	$15.17^{+0.12}_{-0.11}$

FSUGold [47] models. These two interactions systematically overestimate the centroid energy about 1.2 and 0.7 MeV, respectively. On the other hand, from the Skyrme-QRPA calculation of Cao *et al.* [48] with parameter sets SkP [49], SkM\* [50], and Sly5 [51] we can learn that the nonrelativistic Skyrme model predicts a relatively smaller centroid energy, especially in SkP case; the position of GMR peaks are even underestimated by 0.3–0.4 MeV.

The incompressibility of the nonlinear covariant models NL3 and FSUGold are 271 and 229 MeV [52], respectively, while that for Skyrme sets SkP, SkM\*, and Sly5 are 202, 217, and 230 MeV, respectively [48]. The relative shifts of GMR peaks predicted by those interactions manifest the fact that the incompressibility modulus is closely correlated with the centroid of monopole resonance. The density-dependent covariant meson-exchange model DD-ME2 has a incompressibility about 251 MeV [52]; therefore, the shifts in our calculations are reasonable.

When evaluating the GMR energies, there's a challenging problem, i.e., the “softness” of Sn isotopes [53–56], which describes such a situation that the theoretical models producing GMR energies of  $^{208}\text{Sn}$  and  $^{90}\text{Zr}$  correctly will overestimate that of Sn isotopes. It has been shown that the same problem exists in Cd isotopes, too [44]. The theoretical prediction of GMR energies in Cd isotopes by the interactions well calibrated in  $^{208}\text{Pb}$  are systematically larger than experimental results. From the comparison in Table II it is clear that the parameter set SkM\* of the Skyrme interaction shows the best performance in producing the GMR energies of Cd isotopes. However, the centroid energy of the GMR in  $^{208}\text{Pb}$  is better described with the nonrelativistic Sly5 parameter set or relativistic interaction DD-ME2, which we adopted in the current calculation. The ISGMR of  $^{208}\text{Pb}$  are presented in Fig. 3. The dashed-dotted and dashed curves are generated from a Skyrme-RPA solver developed by Colò *et al.* [57] with parameter sets Sly5 and SkM\*, respectively. The centroid energies of  $^{208}\text{Pb}$  reproduced by these two interactions are 13.92 and 13.50 MeV. The former, Sly5, is in good agreement with experimental result  $14.17 \pm 0.28$  MeV [58] while the latter, SkM\*, underestimated. Our FAM calculation (denoted by a solid line) shows the relativistic meson-exchange interaction DD-ME2 will produce the desired GMR energy for  $^{208}\text{Pb}$ , which is about 13.93 MeV and very close to Sly5, but overestimates that for Cd isotopes, too.

The theoretical prediction of the GMR strength distribution has a significant deficiency in energy region 20–30 MeV when compared with experimental observations; there's a fat tail found in cadmium isotopes experimentally. This problem has also been found in other RPA/QRPA calculations [44,48], both

from a relativistic view and from a nonrelativistic view, with pairing or without pairing. Therefore, we believe that to explain the fat tail the extensions beyond the mean field or theory breakthrough of random phase approximation method may be required.

### B. Electric dipole resonance of $^{60}\text{Ni}$

The implementation of a FAM through the direct variation approach can be extended to the calculation of multiple excitation with  $K^\pi \neq 0^+$  easily. As a simple example, we calculate the electric dipole resonance of  $^{60}\text{Ni}$ . The electric dipole excitation is characterized by the operator [59]

$$\hat{E}_{1\mu} = \frac{Ne}{N+Z} \sum_{p=1}^Z r_p Y_{1\mu} - \frac{Ze}{N+Z} \sum_{n=1}^N r_n Y_{1\mu}. \quad (47)$$

Under axial symmetry, the  $E1$  operator involves  $K^\pi = 0^-$  and  $K^\pi = 1^-$  channels (the transition strength that belongs to the  $K = -1$  channel is identical to  $K = 1$ ; therefore, we just need double the contribution of the  $K = 1$  channel when calculating the whole strength distribution). From Fig. 4 we can see, in this oblate deformed nucleus ( $\beta \approx -0.15$ ), transition strength belonging to  $K^\pi = 0^-$  and  $K^\pi = 1^-$  split (represented by the dashed line and dotted-dashed line, respectively), which makes the total strength distribution fragmented in a wide range. Apart from the wide structure of the giant dipole resonance, we can observe a small peak under 10 MeV, which is often referred as pygmy dipole resonance (PDR) [60,61]. This low-lying  $E1$  strength is usually explained as the excess neutrons oscillating against the isospin saturated core [62–64].

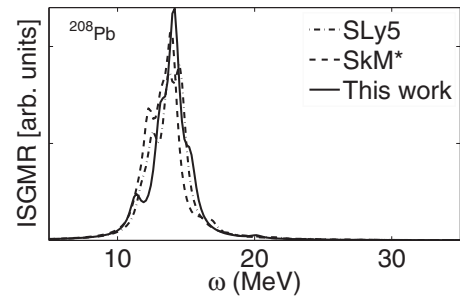


FIG. 3. ISGMR of  $^{208}\text{Pb}$ ; the “dashed-dotted” and “dashed” lines represent results produced by Skyrme interactions Sly5 and SkM\*, respectively. The “solid” line represents our calculation result with relativistic meson-exchange interaction DD-ME2. The response strength is smeared with  $\Gamma = 1$  MeV.

TABLE III. The comparison of the GDR and PDR; the energy is in units of MeV. The fifth column contains the percentage of the TRK sum rule exhausted by the PDR and GDR.

	$E_{\text{cen}}$	$E_{\text{con}}$	$E_{\text{sca}}$	$\sum m_k^1/S(\text{TRK})$
PDR	8.14	8.02	8.44	0.74%
GDR	20.77	19.90	23.36	104%

The classical Thomas-Reiche-Kuhn (TRK) sum rule is model independent and can be evaluated through nucleus mass number [59]

$$S(\text{TRK}) = \sum_n \hbar \omega_n |\langle n | \hat{E}_{1\mu} | g.s. \rangle|^2 = \frac{\hbar^2}{2M} \frac{9}{4\pi} \frac{NZ}{A} e^2 \approx 14.9 \frac{NZ}{A} e^2. \quad (48)$$

Just like the name indicates, the pygmy dipole resonance usually takes a small percentage of the classical EWSR. In our calculation, the value is about 0.74%, while the giant dipole resonance take a large percentage of the EWSR, about 104%. In Table III, we compare the giant dipole resonance (GDR) and PDR about several moment ratios, namely, the centroid energy  $E_{\text{cen}} = m_1/m_0$  as well as the constrained energy  $E_{\text{con}} = \sqrt{m_1/m_{-1}}$  and the scaling energy  $E_{\text{sca}} = \sqrt{m_3/m_1}$ . The energy region is restricted to  $5 < \omega < 10$  MeV when calculating various customary moments for the PDR, and  $10 < \omega < 30$  MeV for GDR. The GDR peak is severely fragmented; there's a remarkable difference between the constrain energy  $E_{\text{con}}$  and scaling energy  $E_{\text{sca}}$ . While for the PDR, the peak is concentrated at about 8 MeV.

Scheck *et al.* [65] investigated the excited behavior of  $^{60}\text{Ni}$  in a  $(\gamma, \gamma')$  reaction, in which the excited states belonging to pygmy resonance are identified by their decay patterns. The experiment shows there's a local accumulation of strong  $E1$  excitations near 8 MeV. This result is close to our FAM-QRPA calculation with a centroid energy about 8.14 MeV in the PDR energy region.

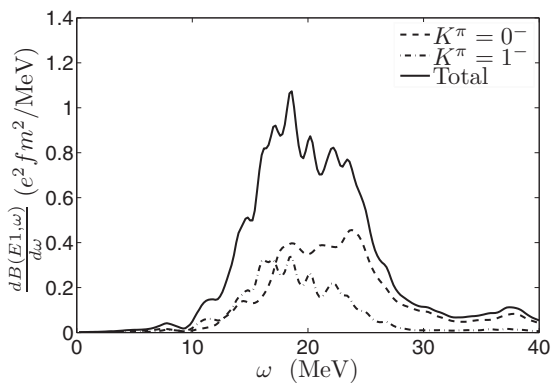


FIG. 4. The electric dipole resonance of  $^{60}\text{Ni}$ . Strength distribution belonging to  $K^\pi = 0^-$  and  $K^\pi = 1^-$  are represented by the dashed line and dotted-dashed line, respectively.

## V. CONCLUSION

A finite-amplitude method is efficient to deal with RPA/QRPA problems with large configuration space. It frees one from the tedious procedure of calculating residual interaction matrix elements; meanwhile, it avoids the huge storage memory and time-consuming diagonalization. By solving the linear response equation iteratively, one gets the transition densities at a given frequency. The processes corresponding to different excitation energies are independent, which make the method suitable for parallel calculation.

In this work, we have fulfilled the implementation of a finite-amplitude method in the relativistic meson exchange mean field model with axial symmetry. The mean field is described by exchanging medium mesons and photons, and the pairing effect is treated in a self-consistent way through relativistic Hartree-Bogoliubov framework. In our FAM-QRPA implementation, the finite difference parameter  $\eta$  is not required; instead, the explicit form of the Hamiltonian variation  $\delta h$  is deduced. This makes our formalism capable of being applied to the  $K^\pi \neq 0^+$  case.

As applications, we have used our program to calculate the giant monopole resonance in cadmium isotopes and electric dipole resonance of  $^{60}\text{Ni}$ . In the latter case, we found a prominent peak of the pygmy dipole resonance centered about 8.14 MeV; this is in good agreement with the experimental result. While in the former case, the position of GMR peaks are slightly larger than those predicted by nonrelativistic Skyrme-QRPA models. The reason is mainly because the incompressibility of the interaction we used, as well as other relativistic nonlinear meson-exchange interactions, is relatively larger than Skyrme ones. Moreover, there's a deficiency of theoretical prediction compared with experimental curves in the high energy region, no matter whether the framework is relativistic or nonrelativistic. The failure to reproduce the fat tail of experimental curves in the cadmium isotopes monopole resonance from the RPA/QRPA view may imply the necessary extension of the current theory scheme, such as extend the scheme of one-particle one-hole (1p1h) or two-quasiparticle (2qp) excitation modes to multi-particle-multi-hole (NpNh) or multi-quasiparticle (Nqp) corrections, including the correlation between single particle motion and collective excitations.

The FAM framework we established in the axial relativistic meson-exchange model with density dependent coupling makes it possible to study the multipole excitation of a wide range of deformed nuclei through a self-consistent approach with mild numerical costs. In future investigation we'd like to extend our method to the triaxial deformed case, which will enable the study of nuclei with large triaxial quadrupole shapes, such as  $^{62}\text{Zn}$ ,  $^{106}\text{Ru}$ ,  $^{134}\text{Ce}$ , etc. This is essential for a systematic investigation of PDR evolution. A previous work has been fulfilled by Inakura *et al.* [8] with a Skyrme-FAM in the absence of pairing, and valuable results have been achieved. It's interesting to check whether pairing interaction and relativistic treatment will introduce new corrections. Meanwhile, in order to settle the problem of "soft" GMR energies in Sn/Cd isotopes completely, it's meaningful to launch a systematic investigation to find out in what range

of the periodic table the GMR energies is overestimated or underestimated. This will shed light upon how theoretical models should be improved.

### ACKNOWLEDGMENTS

We wish to acknowledge the computer resource support provided by the Institute for Fusion Theory and Simulation (IFTS) of Zhejiang University.

### APPENDIX A: THE DEFORMED HARMONIC OSCILLATOR BASIS

The wave function of the harmonic oscillator basis can be found in [66]; for convenience, we list the result here. The basis in the radial direction is expressed as generalized Laguerre polynomials

$$\phi_{n_r}^{m_l}(r_\perp) = \frac{\mathcal{N}_{n_r}^{m_l}}{b_\perp} \sqrt{2\eta} L_{n_r}^{m_l}(\eta) e^{-\eta/2}, \quad (\text{A1})$$

and in the  $z$  direction, Hermite polynomials

$$\phi_{n_z}(z) = \frac{\mathcal{N}_{n_z}}{\sqrt{b_z}} H_{n_z}(\zeta) e^{-\zeta^2/2}, \quad (\text{A2})$$

where  $b_z$  and  $b_\perp$  are oscillator lengths and  $\zeta$  and  $\eta$  are dimensionless variables

$$\zeta = z/b_z, \quad \eta = r_\perp^2/b_\perp^2. \quad (\text{A3})$$

The normalization constants of Hermite and Laguerre polynomials are

$$\mathcal{N}_{n_z} = \frac{1}{\sqrt{\sqrt{\pi} 2^{n_z} n_z!}} \quad \text{and} \quad \mathcal{N}_{n_r}^{m_l} = \sqrt{\frac{n_r!}{(n_r + m_l)!}}. \quad (\text{A4})$$

The eigenfunction of the deformed oscillator is

$$\Phi_\alpha(\mathbf{r}, s, t) = \frac{e^{im_l\varphi}}{\sqrt{2\pi}} \phi_{n_r}^{m_l}(r_\perp) \phi_{n_z}(z) \chi_{m_s}(s) \chi_{m_l}(t). \quad (\text{A5})$$

In the axial symmetry condition, the electric dipole operator (47) can be expressed as

$$\hat{E}_{11} = -\frac{e_{\text{eff}}}{\sqrt{2}} r_\perp e^{i\varphi}, \quad \hat{E}_{10} = e_{\text{eff}} z, \quad (\text{A6})$$

with effective charges defined by

$$e_{\text{eff}} = \begin{cases} +\frac{eN}{A}, & \text{proton} \\ -\frac{eZ}{A}, & \text{neutron.} \end{cases} \quad (\text{A7})$$

The matrix elements of the electric dipole operator in basis (A5) are

$$\langle \alpha' | \hat{E}_{11} | \alpha \rangle = -\frac{b_\perp e_{\text{eff}}}{\sqrt{2}} \delta_{m'_l, m_l+1} \delta_{m'_s, m_s} \delta_{n'_z, n_z} \times G(n'_r, m'_l, n_r, m_l, +1), \quad (\text{A8})$$

$$\langle \alpha' | \hat{E}_{10} | \alpha \rangle = b_z e_{\text{eff}} \delta_{m'_l, m_l} \delta_{m'_s, m_s} \delta_{n'_r, n_r} \times (n_z \delta_{n'_z, n_z-1} + \frac{1}{2} \delta_{n'_z, n_z+1}) \mathcal{N}_{n_z} / \mathcal{N}_{n'_z}, \quad (\text{A9})$$

where  $G$  is the shorthand for the Laguerre polynomials integral

$$\begin{aligned} G(n'_r, m'_l, n_r, m_l, b) &= \mathcal{N}_{n'_r}^{m'_l} \mathcal{N}_{n_r}^{m_l} \int_0^\infty z^\lambda e^{-z} L_{n'_r}^{m'_l}(z) L_{n_r}^{m_l}(z) dz \\ &= \mathcal{N}_{n'_r}^{m'_l} \mathcal{N}_{n_r}^{m_l} (-)^{n'_r+n_r} \Gamma(\lambda+1) \sum_k C_{\lambda-m'_l}^{n'_r-k} C_{\lambda-m_l}^{n_r-k} C_{\lambda+k}^k, \end{aligned} \quad (\text{A10})$$

with  $\lambda = \frac{m'_l + m_l + b}{2}$ .

As for the matrix elements of monopole operator (46), we refer to the Appendix of [13].

### APPENDIX B: THE VARIATION OF COUPLING CONSTANTS

In order to improve the behavior of the EOS (equation of state) in the high energy region, the coupling parameters of nucleon-meson interaction are set to be density dependent. In the model we used, the explicit density dependence form of nucleon-meson coupling constants are

$$g_i(\rho) = g_i(\rho_{\text{sat}}) f_i(x) \quad \text{for } i = \sigma, \omega, \quad (\text{B1})$$

where  $\rho_{\text{sat}}$  is the saturation baryon density in symmetric nuclear matter, and  $x = \rho/\rho_{\text{sat}}$  is the relative density. The function  $f$  has the form

$$f_i(x) = a_i \frac{1 + b_i(x + d_i)^2}{1 + c_i(x + d_i)^2} \quad (\text{B2})$$

for  $\sigma, \omega$  mesons, and

$$g_\rho = g_\rho(\rho_{\text{sat}}) e^{-a_\rho(x-1)} \quad (\text{B3})$$

for  $\rho$  meson. The value of these coupling parameters in a DD-ME2 model can be found in [38]. Under a small amplitude approximation, the variation of coupling constants induced by the transition density can be expressed as

$$\begin{aligned} \delta g_i(\rho) &= \frac{g_i(\rho_{\text{sat}})}{\rho_{\text{sat}}} \left. \frac{\partial f_i}{\partial x} \right|_0 \delta\rho, \\ \delta \frac{\partial g_i(\rho)}{\partial \rho} &= \frac{g_i(\rho_{\text{sat}})}{\rho_{\text{sat}}^2} \left. \frac{\partial^2 f_i}{\partial x^2} \right|_0 \delta\rho, \end{aligned} \quad (\text{B4})$$

with derivatives

$$\begin{aligned} \frac{\partial f_{\sigma, \omega}}{\partial x} &= \frac{2a(b-c)(x+d)}{[1+c(x+d)^2]^2}, \\ \frac{\partial^2 f_{\sigma, \omega}}{\partial x^2} &= 2a(b-c) \frac{1-3c(x+d)^2}{[1+c(x+d)^2]^3}, \\ \frac{\partial f_\rho}{\partial x} &= -a_\rho e^{-a_\rho(x-1)}, \quad \frac{\partial^2 f_\rho}{\partial x^2} = a_\rho^2 e^{-a_\rho(x-1)}. \end{aligned} \quad (\text{B5})$$

- [1] K. Yoshida and N. V. Giai, *Phys. Rev. C* **78**, 064316 (2008).
- [2] C. Losa, A. Pastore, T. Døssing, E. Vigezzi, and R. A. Broglia, *Phys. Rev. C* **81**, 064307 (2010).
- [3] J. Terasaki and J. Engel, *Phys. Rev. C* **82**, 034326 (2010).
- [4] K. Yoshida and T. Nakatsukasa, *Phys. Rev. C* **83**, 021304 (2011).
- [5] D. Pena Arteaga and P. Ring, *Phys. Rev. C* **77**, 034317 (2008).
- [6] T. Nakatsukasa, T. Inakura, and K. Yabana, *Phys. Rev. C* **76**, 024318 (2007).
- [7] T. Inakura, T. Nakatsukasa, and K. Yabana, *Phys. Rev. C* **80**, 044301 (2009).
- [8] T. Inakura, T. Nakatsukasa, and K. Yabana, *Phys. Rev. C* **84**, 021302 (2011).
- [9] H. Liang, T. Nakatsukasa, Z. Niu, and J. Meng, *Phys. Rev. C* **87**, 054310 (2013).
- [10] P. Avogadro and T. Nakatsukasa, *Phys. Rev. C* **84**, 014314 (2011).
- [11] M. Stoitsov, M. Kortelainen, T. Nakatsukasa, C. Losa, and W. Nazarewicz, *Phys. Rev. C* **84**, 041305 (2011).
- [12] T. Nikšić, D. Vretenar, and P. Ring, *Phys. Rev. C* **78**, 034318 (2008).
- [13] T. Nikšić, N. Kralj, T. Tutiš, D. Vretenar, and P. Ring, *Phys. Rev. C* **88**, 044327 (2013).
- [14] T. Nakatsukasa, K. Matsuyanagi, M. Matsuo, and K. Yabana, *Rev. Mod. Phys.* **88**, 045004 (2016).
- [15] B. Carlsson, J. Dobaczewski, J. Toivanen, and P. Veselý, *Comput. Phys. Commun.* **181**, 1641 (2010).
- [16] B. G. Carlsson, J. Dobaczewski, and M. Kortelainen, *Phys. Rev. C* **78**, 044326 (2008).
- [17] B. G. Carlsson, J. Toivanen, and A. Pastore, *Phys. Rev. C* **86**, 014307 (2012).
- [18] M. Stoitsov, J. Dobaczewski, W. Nazarewicz, and P. Ring, *Comput. Phys. Commun.* **167**, 43 (2005).
- [19] M. Stoitsov, N. Schunck, M. Kortelainen, N. Michel, H. Nam, E. Olsen, J. Sarich, and S. Wild, *Comput. Phys. Commun.* **184**, 1592 (2013).
- [20] N. Hinohara, M. Kortelainen, and W. Nazarewicz, *Phys. Rev. C* **87**, 064309 (2013).
- [21] M. Kortelainen, N. Hinohara, and W. Nazarewicz, *Phys. Rev. C* **92**, 051302 (2015).
- [22] K. Bennaceur and J. Dobaczewski, *Comput. Phys. Commun.* **168**, 96 (2005).
- [23] P. Avogadro and T. Nakatsukasa, *Phys. Rev. C* **87**, 014331 (2013).
- [24] J. C. Pei, M. V. Stoitsov, G. I. Fann, W. Nazarewicz, N. Schunck, and F. R. Xu, *Phys. Rev. C* **78**, 064306 (2008).
- [25] J. C. Pei, M. Kortelainen, Y. N. Zhang, and F. R. Xu, *Phys. Rev. C* **90**, 051304 (2014).
- [26] M. T. Mustonen, T. Shafer, Z. Zenginerler, and J. Engel, *Phys. Rev. C* **90**, 024308 (2014).
- [27] J. G. Valatin, *Phys. Rev.* **122**, 1012 (1961).
- [28] P. Ring and P. Schuck, *The Nuclear Many-Body Problem* (Springer-Verlag Inc., New York, 2004).
- [29] D. Vretenar, A. Afanasjev, G. Lalazissis, and P. Ring, *Phys. Rep.* **409**, 101 (2005).
- [30] C. Fuchs, H. Lenske, and H. H. Wolter, *Phys. Rev. C* **52**, 3043 (1995).
- [31] P. Ring, Z. yu Ma, N. V. Giai, D. Vretenar, A. Wandelt, and L.-g. Cao, *Nucl. Phys. A* **694**, 249 (2001).
- [32] D. Vautherin, *Phys. Rev. C* **7**, 296 (1973).
- [33] M. Serra and P. Ring, *Phys. Rev. C* **65**, 064324 (2002).
- [34] T. Nikšić, N. Paar, D. Vretenar, and P. Ring, *Comput. Phys. Commun.* **185**, 1808 (2014).
- [35] Y. Tian, Z. Ma, and P. Ring, *Phys. Lett. B* **676**, 44 (2009).
- [36] M. A. Rashid, *J. Phys. A: Math. Gen.* **13**, 1977 (1980).
- [37] L. Chaos-Cador and E. Ley-Koo, *Int. J. Quantum Chem.* **97**, 844 (2004).
- [38] G. A. Lalazissis, T. Nikšić, D. Vretenar, and P. Ring, *Phys. Rev. C* **71**, 024312 (2005).
- [39] Y. Tian, Z.-y. Ma, and P. Ring, *Phys. Rev. C* **79**, 064301 (2009).
- [40] D. D. Johnson, *Phys. Rev. B* **38**, 12807 (1988).
- [41] A. Baran, A. Bulgac, M. McNeil Forbes, G. Hagen, W. Nazarewicz, N. Schunck, and M. V. Stoitsov, *Phys. Rev. C* **78**, 014318 (2008).
- [42] N. Paar, P. Ring, T. Nikšić, and D. Vretenar, *Phys. Rev. C* **67**, 034312 (2003).
- [43] J. Blaizot, *Phys. Rep.* **64**, 171 (1980).
- [44] D. Patel, U. Garg, M. Fujiwara, H. Akimune, G. Berg, M. Harakeh, M. Itoh, T. Kawabata, K. Kawase, B. Nayak, T. Ohta, H. Ouchi, J. Piekarewicz, M. Uchida, H. Yoshida, and M. Yosoi, *Phys. Lett. B* **718**, 447 (2012).
- [45] Y.-W. Lui, D. H. Youngblood, Y. Tokimoto, H. L. Clark, and B. John, *Phys. Rev. C* **69**, 034611 (2004).
- [46] G. A. Lalazissis, J. König, and P. Ring, *Phys. Rev. C* **55**, 540 (1997).
- [47] B. G. Todd-Rutel and J. Piekarewicz, *Phys. Rev. Lett.* **95**, 122501 (2005).
- [48] L.-G. Cao, H. Sagawa, and G. Colò, *Phys. Rev. C* **86**, 054313 (2012).
- [49] J. Dobaczewski, H. Flocard, and J. Treiner, *Nucl. Phys. A* **422**, 103 (1984).
- [50] J. Bartel, P. Quentin, M. Brack, C. Guet, and H.-B. Håkansson, *Nucl. Phys. A* **386**, 79 (1982).
- [51] E. Chabanat, P. Bonche, P. Haensel, J. Meyer, and R. Schaeffer, *Nucl. Phys. A* **635**, 231 (1998).
- [52] B.-A. Li, L.-W. Chen, and C. M. Ko, *Phys. Rep.* **464**, 113 (2008).
- [53] J. Piekarewicz, *Phys. Rev. C* **76**, 031301 (2007).
- [54] U. Garg, T. Li, S. Okumura, H. Akimune, M. Fujiwara, M. Harakeh, H. Hashimoto, M. Itoh, Y. Iwao, T. Kawabata, K. Kawase, Y. Liu, R. Marks, T. Murakami, K. Nakanishi, B. Nayak, P. M. Rao, H. Sakaguchi, Y. Terashima, M. Uchida, Y. Yasuda, M. Yosoi, and J. Zenihiro, *Proceedings of the 2nd International Conference on Collective Motion in Nuclei under Extreme Conditions, 2006, St. Goar, Germany* [*Nucl. Phys. A* **788**, 36 (2007)],
- [55] J. Piekarewicz, *J. Phys. G: Nucl. Particle Phys.* **37**, 064038 (2010).
- [56] T. Li, U. Garg, Y. Liu, R. Marks, B. K. Nayak, P. V. Madhusudhana Rao, M. Fujiwara, H. Hashimoto, K. Kawase, K. Nakanishi, S. Okumura, M. Yosoi, M. Itoh, M. Ichikawa, R. Matsuo, T. Terazono, M. Uchida, T. Kawabata, H. Akimune, Y. Iwao, T. Murakami, H. Sakaguchi, S. Terashima, Y. Yasuda, J. Zenihiro, and M. N. Harakeh, *Phys. Rev. Lett.* **99**, 162503 (2007).
- [57] G. Colò, L. Cao, N. V. Giai, and L. Capelli, *Comput. Phys. Commun.* **184**, 142 (2013).
- [58] D. H. Youngblood, H. L. Clark, and Y.-W. Lui, *Phys. Rev. Lett.* **82**, 691 (1999).
- [59] B. R. Mottelson and A. N. Bohr, *Nuclear Structure* (World Scientific Pub. Co., Inc., Singapore, 1998), two volume set.
- [60] J. S. Brzosko, E. Gierlik, A. Soltan, Jr., and Z. Wilhelmi, *Can. J. Phys.* **47**, 2849 (1969).

- [61] N. Paar, D. Vretenar, E. Khan, and G. Colò, *Rep. Prog. Phys.* **70**, 691 (2007).
- [62] P. G. Hansen and B. Jonson, *Europhys. Lett.* **4**, 409 (1987).
- [63] Y. Suzuki and Y. Tosaka, *Nucl. Phys. A* **517**, 599 (1990).
- [64] D. Vretenar, N. Paar, P. Ring, and G. Lalazissis, *Nucl. Phys. A* **692**, 496 (2001).
- [65] M. Scheck, V. Y. Ponomarev, T. Aumann, J. Beller, M. Fritzsche, J. Isaak, J. H. Kelley, E. Kwan, N. Pietralla, R. Raut, C. Romig, G. Rusev, D. Savran, K. Sonnabend, A. P. Tonchev, W. Tornow, H. R. Weller, and M. Zweidinger, *Phys. Rev. C* **87**, 051304 (2013).
- [66] P. Ring, Y. Gambhir, and G. Lalazissis, *Comput. Phys. Commun.* **105**, 77 (1997).